Surface-functionalized Boron Nanoparticles with Reduced Oxide Content by Non-thermal Plasma Processing for Nanoenergetic Applications

Prawal P.K. Agarwal[1], Devon Jensen[2], Chien-Hua Chen[2], Robert M. Rioux[1,3], Themis Matsoukas[1]*

[1]Department of Chemical Engineering, The Pennsylvania State University, University Park, Pennsylvania, United States

[2]Advanced Cooling Technologies, Inc., Lancaster, Pennsylvania 17601, United States

[3]Department of Chemistry, The Pennsylvania State University, University Park, Pennsylvania, United States

*E-mail of Corresponding Author: txm11@psu.edu

Table of Contents (TOC)

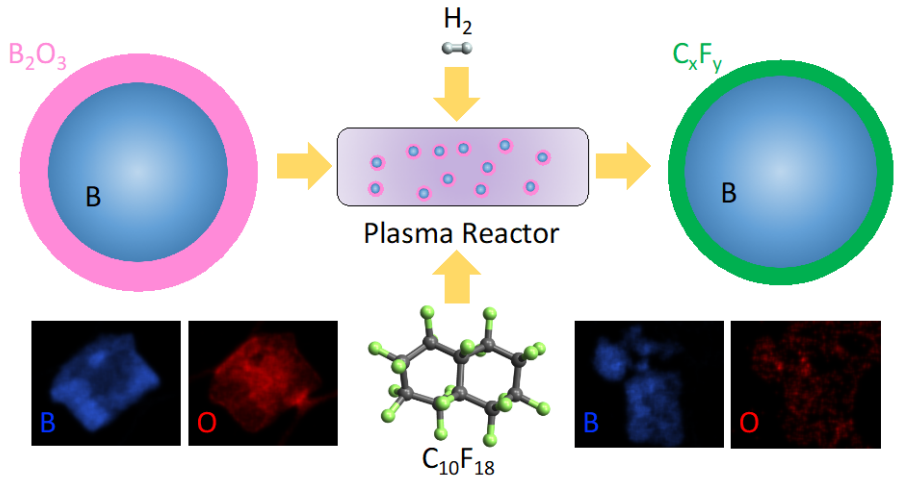

ABSTRACT

The development of an *in-situ* non-thermal plasma technology improved the oxidation and energy release of boron nanoparticles. We reduced the native oxide layer on the surface of boron nanoparticles (70 nm) by treatment in a non-thermal hydrogen plasma, followed by the formation of a passivation barrier by argon plasma-enhanced chemical vapor deposition (PECVD) using perfluorodecalin ($C_{10}F_{18}$). Both processes occur near room temperature, thus avoiding aggregation and sintering of the nanoparticles. HR-TEM, HAADF-STEM-EDS, and XPS demonstrated a significant reduction in surface oxide concentration due to hydrogen plasma treatment and the formation of a 2.5 nm thick passivation coating on the surface due to PECVD treatment. These results correlated with the thermal analysis results, which demonstrated a 19% increase in energy release and an increase in metallic boron content after 120 min of hydrogen plasma treatment and 15 min of PECVD of perfluorodecalin. The PECVD coating provided excellent passivation against air and humidity for 60 days. We conclude *in-situ* non-thermal plasma reduction and passivation lead to the amelioration of energy release characteristics and storage life of boron nanoparticles, benefits conducive for nanoenergetic applications.

KEYWORDS: boron, hydrogen plasma, native oxide, energy release, nanoenergetic materials, PECVD

1. INTRODUCTION

Metal nanoparticles have great potential as additives to liquid and solid fuels and even as fuels themselves since they oxidize readily, release large amounts of heat while producing no greenhouse gas emissions [1-6]. Compared to liquid fuels, the volumetric energy content of metals is much higher. It has been estimated a vehicle that utilizes aluminum as a fuel would cover three times the distance without refueling compared to a vehicle running on gasoline [5]. Current research focuses on their use as a secondary fuel in volume-limited propulsion to improve the energy efficiency of existing engines without adversely impacting other fuel properties such as freezing point, flash point, and viscosity [3,4,7-10]. Nanometer-sized particles are especially advantageous. They exhibit high reactivity, lower melting points, enhanced heat and mass transfer properties, lower sintering temperatures and faster heat release as compared to micron and larger-sized particles, and better overall combustion characteristics [3,4-6]. Thus, it is possible to improve the performance of conventional liquid fuels by the addition of rather small amounts of energetic nanomaterials. Maintaining the low volume fraction of solids is important to utilize the fuel without the need to modify the engine [1,2]. On the other hand, new challenges arise when the particle size is too small. The main limitation is due to the presence of the native oxide layer. While this layer provides passivation during storage, for nanometer-size particles it represents a significant fraction of the particle mass. Additionally, nanoparticles are prone to aggregation, leading to unstable dispersions that cause precipitation, deposition on pipe walls, and pump erosion during fuel transportation [3,11-13].

Aluminum, boron, copper, iron, and magnesium are among the most extensively studied energetic materials [3-8]. Boron is of particular interest because of its exceptionally high gravimetric (58 kJ/g) and volumetric (140 kJ/mL) energy densities [10,14], which are much greater than hydrocarbon fuels (~25-40 kJ/g) [1,5], explosives (~10-15 kJ/g), and other high energy density metals like magnesium (25 kJ/g) and aluminum (31 kJ/g) [1,3]. Boron has

applications in various fields including medicine (mineral for building strong bones) [15-16], military (aircraft, missiles, and other specialized weapons) [2,3,10], protective coatings [17], and semiconductors [18]. Several studies demonstrated the liquid-phase and vapor-phase synthesis of boron nanoparticles (BNPs) [14], but they were unable to circumvent the formation of a native oxide layer [19-27]. The main impediment in the application of boron nanoparticles is the reduced energy output and lagged combustion reaction kinetics due to the formation of a native oxide shell that acts as a barrier to further oxidation of the core [10, 14, 28-30]. Strong reducing agents such as hydrogen and carbon may be used to reduce oxide, but the reaction is thermodynamically infeasible even at very high temperatures [31-32]. Hydrogen plasma, through either thermal or non-thermal routes, can be used to reduce the thickness of the native oxide layer [31]. Non-thermal plasma offers inherent thermodynamic and kinetic advantages for the reduction of metal oxide due to the formation of highly reactive atomic and ionic species at low temperatures [31-32]. Non-thermal hydrogen plasma has been shown to successfully remove the native oxide layer from germanium, copper, silicon, and ruthenium surfaces [33-36]. Hydrogen plasma can reduce almost every metal oxide at low temperatures because of the highly negative Gibbs energy change [31]. The driving force for reduction is the formation of highly reactive hydrogen atoms, ions, and vibrationally excited hydrogen molecules that react with the oxide layer at the plasma-boron oxide interface leading to the reduction reaction forming elemental boron and water vapor with a highly negative Gibbs energy at 298 K for atomic hydrogen [31]. The low temperature of non-thermal hydrogen plasma enables native oxide removal without the sintering of nanoparticles.

In the absence of the oxide layer, the boron surface re-oxidizes rapidly upon contact with air and moisture [10]. Passivation by surface functionalization or encapsulation is necessary to prevent re-oxidation [11-13]. BNPs have been functionalized using alkoxy groups, halogens, silanes, organic acid, and polymers [14,26,28]. A simple synthesis route of

functionalized BNPs at room temperature was suggested by Pickering et al. [28]. Boron tribromide was reduced to form a sticky, pale yellow compound rich in boron followed by a reaction with excess octanol to produce octyloxy-capped BNPs. Gas-phase pyrolysis of decaborane followed by surface functionalization with halides (Br and F) was studied by Bellott et al. [26]. Passivation of BNPs against oxidation is possible at the cost of reduced energy release as suggested by their thermal analysis results. The energy release decreased by 18% and 2% after forming F and Br capping respectively. This decrease is the result of the chemical bonding of the boron surface with halogens, which reduces the percentage of metallic boron available for the oxidation reaction. Shin et al. synthesized BNPs in the range of ~30-70 nm by gas-phase nucleation of BCl_3 by rapid expansion through a nozzle within a thermal plasma [30]. As-made particles were metallic boron with a hydride layer on the surface, but under storage in ambient air, oxidation occurred and the thickness of the oxide layer stabilized within two days. A different approach was used by Devener et al. [14] to produce air-stable boron with low oxide content. High energy ball milling was used to reduce the size of commercial micron-sized boron particles down to ~50 nm in the presence of oleic acid. Size reduction exposes boron on the particle surface and even though the oxide itself is not removed, fine particles are highly enriched in metallic boron. It was shown that capping with oleic acid was successful in producing air-stable BNPs with no measurable oxygen at the detection limit of XPS. Recently, Chintersingh et al. [37] reported a method to remove the hydrated surface oxide from the surface of boron particles by washing them in acetonitrile with and without hydrocarbon fluids. They observed that the resulting boron powder displayed shorter ignition delays as compared to starting commercial boron powder. Combustion characteristics of the boron powder remained unaffected after this modification process. Valluri et al. [38] studied double displacement, salt metathesis reaction between boron and bismuth fluoride to passivate the surface of boron. The experimental results suggested that ignition temperature for the

oxidation of the material was reduced after the employment of the bismuth fluoride coating. Additionally, single-particle combustion experiments showed an accelerated burn rate from the coated sample as compared to boron. This work demonstrates that the surface functionalization of boron using fluoride-based coatings is an efficient way to optimize its combustion characteristics.

To fully utilize the energy density of BNPs one must address two problems: eliminate the native oxide at the particle surface while protecting the particle from further oxidation under normal storage conditions. Additionally, the passivating agent should not interfere with combustion and should be effective in amounts sufficiently small, such that the volumetric energy density of the particles is not affected. Ideally, the removal of the oxide layer and passivation of the surface should be done in an integrated process that avoids exposure to air, is capable of utilizing commercially available powders, and minimizes the use of chemical reagents. We are presenting a low-pressure plasma process here that accomplishes these goals. Plasma-enhanced chemical vapor deposition (PECVD) is a versatile technique for the fabrication of surface films since it can utilize chemical precursors in any physical form. It is a dry and readily scalable process that does not require post-processing separations [39-43]. The advantage of PECVD lies in its ability to tailor the coating chemistry to control interfacial properties by merely changing the precursor. The deposition of the precursor from the gas phase enables nanometer-level control of the coating through adjustment of the residence time of precursor vapors in the plasma reactor [44-48]. Argon gas is used as a carrier of precursor vapors to the plasma reactor and serves as a plasma generator gas because of its inert nature. The films obtained by PECVD are pinhole-free and the thickness of the deposited film can be controlled via deposition conditions. As a result of the cross-linked architectures, PECVD coatings are chemically, mechanically, and thermally stable [39-40,45-48]. PECVD was shown to prevent the oxidation of freshly synthesized aluminum nanoparticles by Matsoukas

et al. [40]. They observed coatings from precursors such as toluene, isopropanol, and perfluorodecalin (PFD) provided excellent protection against oxidation by air and humidity by imparting hydrophobic properties to the surface of the NPs [45]. The films made from PFD have a water contact angle of 125°, and the coatings formed were observed to provide a hydrophobic barrier against humidity to increase shelf life under normal storage conditions. Here, we report a unique in-situ method in which a non-thermal hydrogen plasma is used to reduce the native oxide layer from the surface of BNPs, and PECVD is used to form a passivation barrier that protects metallic BNPs against oxidation by air and humidity. This method is a dry process that exposes particles to a minimum number of reagents and does not require post-processing operations.

2. MATERIALS AND METHODS

The setup of the non-thermal plasma process is shown in Figure 1. It consists of six main components: a vacuum supply with a liquid nitrogen trap, a 13.56 MHz radiofrequency (RF) generator equipped with a matching box, a tubular glass reactor, a magnetic stirrer, a hydrogen transport system, and an argon-assisted precursor delivery system. A glass flask serves as a bubbler for delivery of the organic vapor, with an inlet connected to an argon supply through a flow controller and an outlet connected to a tubular reactor through a valve. Argon is used as a carrier gas to transport organic precursor vapor into the reactor. The temperature of the glass flask containing the organic precursor was maintained at 50°C by immersing it into a hot water bath. The RF power used for hydrogen plasma and the PECVD treatments were 40 W and 30 W, respectively. The RF power was chosen so that pressure remains at ~0.1 Torr, which is below the critical value (~0.2 Torr) for hydrogen and argon plasma generation (as observed experimentally). The critical value refers to the highest pressure in the designed system at which non-thermal plasma can be generated inside the reactor. Above this value,

temperature control becomes difficult, which shifts the process towards thermal plasma. Before connecting the reactor to the vacuum system, 0.5 grams of BNPs (Nanoshel, Purity: 99.5%, Average Particle Size: 70 nm) were transferred to the reactor using a disposable spatula. To promote uniform exposure of particles to the plasma and to minimize aggregation, a magnetic micro stir bar was placed inside the reactor, and the magnetic stir plate located outside the reactor was set to 100 rpm, which stirred the particles through spinning the stir bar. The tubular reactor was connected to a vacuum pump. A liquid nitrogen trap was used to condense all organic vapors escaping the reactor before entering the pump and contributed to maintaining a low plasma pressure. Check valves between the vacuum pump and reactor were used to control and regulate a high vacuum in the reactor to avoid attrition of the BNPs. Two external electrodes separated 1 inch from each other were used to generate the non-thermal plasma. The plasma formed when the source impedance matched the load impedance through a matching network [45].

BNPs were treated with hydrogen plasma for 60, 85, and 120 minutes (min) at a pressure of ~0.1 Torr. After treatment with the hydrogen plasma, the hydrogen gas valve was turned off, and the argon valve was opened after placement of the glass bubbler containing perfluorodecalin (PFD, Acros Organics, Purity: 90%) in a water bath at 50°C. After generation of the argon plasma, PFD saturated in argon passed through the reactor for the application of a PECVD coating on BNPs for 15 min. Hydrogen plasma treatments were performed for different periods, while PECVD treatment was kept constant with a treatment time of 15 min. This procedure was followed to observe the effect of the hydrogen plasma treatment time on the reduction of the native oxide. After the PECVD process, particles were collected from the reactor and stored under ambient conditions for further characterization. Thermal analyses of the BNPs were done over time to detect any loss in energy release due to oxidation during storage.

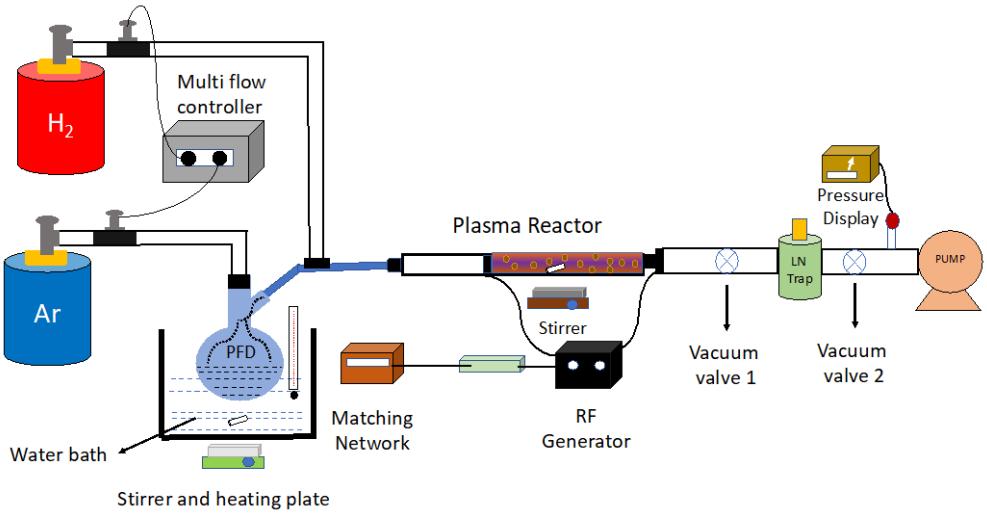

Figure 1. Schematic of the non-thermal plasma setup.

For analysis by transmission electron microscopy (TEM) and scanning TEM (STEM), the particles were dispersed in hexane and sonicated for 10 min with a Branson ultrasonicator (Model: CPX3800H). A few drops of the dispersion were deposited on a TEM lacey carbon copper grid (Electron Microscopy Sciences). Both the TEM and STEM-EDS (Energy Dispersive Spectroscopy) analysis were performed on a Talos F200X at 200 kV with a XFEG source, and an integrated SuperX EDS. It is also equipped with high-angular annular dark-field imaging (HAADF). STEM-EDS provides both qualitative and quantitative information about the elemental composition in the sample. The thicknesses of the organic coating and the surface oxide were estimated by high-resolution TEM (HRTEM) imaging. Scanning electron microscopy (SEM) images were collected on a Zeiss Sigma Variable Pressure (VP) field emission SEM. The BNPs were placed on copper tape for SEM imaging.

X-ray photoelectron spectroscopy (XPS) was employed to obtain the chemical composition and elemental state of the near-surface region of the particles. XPS experiments were performed using a Physical Electronics VersaProbe II instrument equipped with a monochromatic Al kα x-ray source (hν = 1486.7 eV) and a concentric hemispherical analyzer. Charge neutralization was performed using Ar ions and low energy electrons (<5 eV). A take-

off angle of 45° to the sample surface plane was used for all measurements. Quantification was done using instrumental relative sensitivity factors (RSFs) that account for the x-ray cross-section and inelastic mean free path of the electrons [49].

Thermogravimetric analysis and differential scanning calorimetry (TGA/DSC) were performed on a TA Instruments Model Q600 SDT, which provides simultaneous measurement of heat flow and weight change on the same sample from ~20°C to 1400°C. TGA measures the weight gain due to the oxidation of boron, and DSC yields the heat released during the oxidation of active boron. Oxidation tests were conducted in dry air (100 mL/min) for all samples studied. Samples were placed in alumina sample cups (90 μL, TA Instruments). A heating rate of 30°C/min was used up to a maximum temperature of 1400°C.

3. RESULTS

In non-thermal plasma experiments, we varied hydrogen plasma treatment times (0, 60, 85, and 120 min) and the PECVD time was kept constant at 15 min. Characterization experiments, such as TEM, STEM-EDS, and XPS were performed on the samples to analyze the surface oxide composition, both qualitatively and quantitatively. Thermal analysis experiments (TGA and DSC) were also performed on these samples to measure and compare the quantity of metal oxidized and the energy release.

High-resolution Transmission Electron Microscopy (HR-TEM) was performed on the samples to verify the presence of the oxide layer, the PECVD coating, and the reduction in native oxide. High-resolution imaging of BNPs by TEM provided visual evidence of the degree of the oxide removal by hydrogen plasma. Elemental boron and its oxide are distinguished by observation of the lattice spacings of elemental boron and the amorphous nature of the oxide. The PECVD coating at the outer edges of individual particles is characterized by its amorphous nature and lighter contrast as compared to the oxide because of the lower electron density of

the organic coating. In Figure 2, we compare the images of the samples with and without hydrogen plasma treatment keeping a constant 15 min PECVD treatment. Figure 2(a) shows BNPs after 15 min of PECVD treatment but without any hydrogen plasma treatment. These particles carry their native oxide layer which has a thickness of ~6 nm. A thin (~2.5 nm) PECVD coating is observed on top of the oxide surface. Figure 2(b) shows the TEM image of a sample treated in hydrogen plasma for 120 min (the longest hydrogen treatment in this study) followed by 15 min of PECVD treatment. A ~2.5 nm PECVD coating is present but no oxide layer is visible.

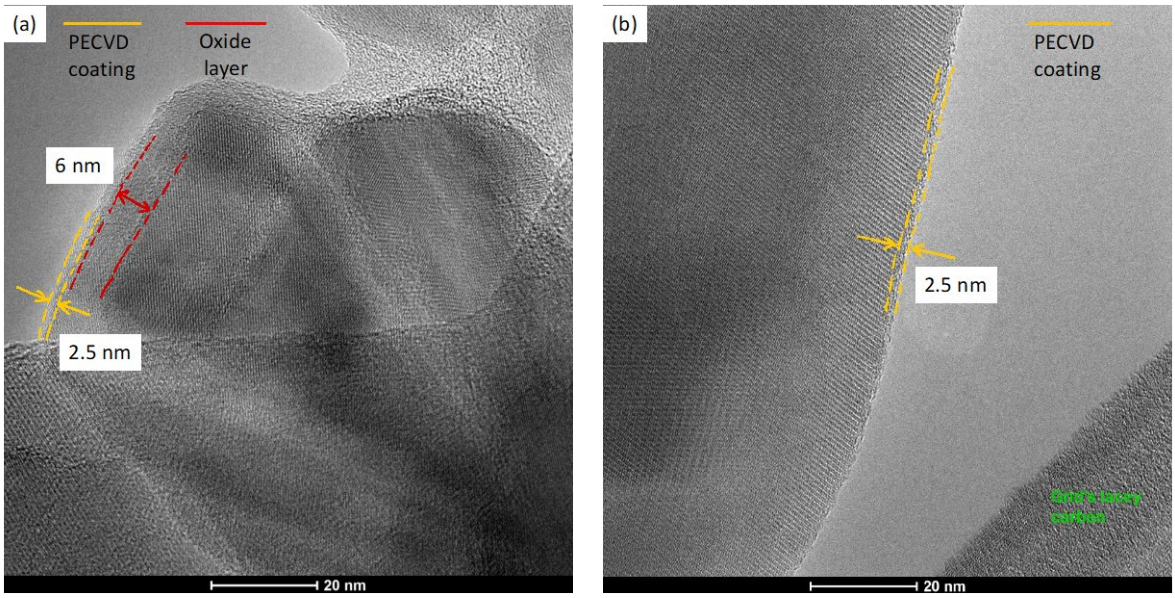

Figure 2. HR-TEM images of BNPs before and after hydrogen plasma treatment (The red line indicates the amorphous oxide layer and the yellow indicates the PECVD coating). (a) No hydrogen plasma treatment and PECVD treatment for 15 min, (b) hydrogen plasma treatment for 120 min and PECVD treatment for 15 min. The scale bar is 20 nm.

The distribution of elements present in the BNPs was studied using Scanning Transmission Electron Microscopy with Energy Dispersive Spectroscopy (STEM-EDS) performed in High Angular Annular Dark Field (HAADF) imaging. The probe depth of EDS is on the order of hundreds of nanometers, much larger than the size of the BNPs (70 nm), thus it provides compositional information over the entire particle. Elemental analysis was quantified in terms of the oxygen-to-boron (O/B) atomic ratio (Figure S3). Figure 3(a) shows

the HAADF-STEM image and 3(b), (c), and (d) exhibit the combined map of boron and oxygen, boron distribution and oxygen distribution, respectively as characterized by EDS. These maps represent the BNPs sample treated for 15 min in PECVD with no hydrogen treatment. The native oxide (red) is seen to surround the boron particles (blue) in the field of view and the O/B atomic ratio in this area is 0.096.

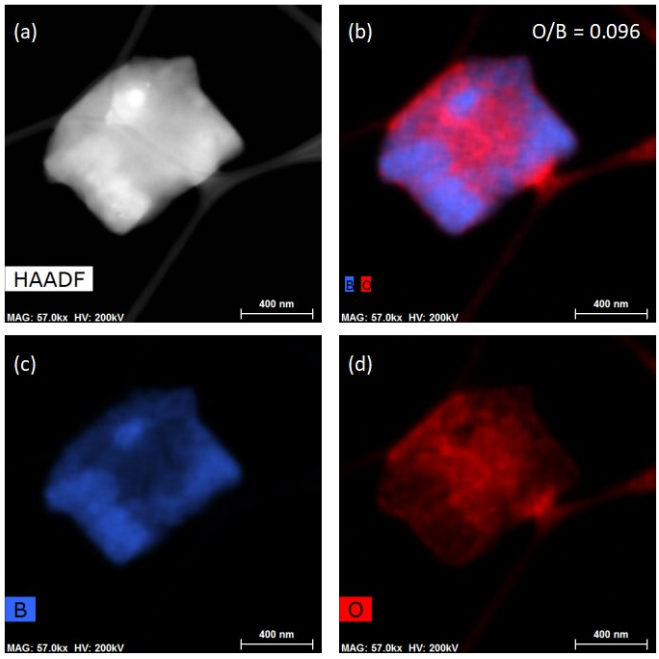

Figure 3. STEM-EDS images of BNPs in HAADF mode before hydrogen plasma treatment. (a) STEM image showing boron particles; (b) EDS image showing the relative distribution of boron (blue) and oxygen (red) on a particle (O/B = 0.096); (c) EDS image showing individual micrograph of boron on a particle; and (d) EDS image showing individual micrograph of oxygen on a particle.

Figure 4(a) shows the HAADF-STEM images and Figures 4(b), (c), and (d) are the combined map of boron and oxygen, boron distribution and oxygen distribution, respectively. These maps represent the BNPs sample treated for 120 min of hydrogen treatment followed by 15 min of PECVD. There is a significant reduction of the oxygen signal and the corresponding O/B ratio decreases to 0.0068, a reduction of more than 90% due to hydrogen plasma treatment. On the other hand, the fluorine signal remains constant as both samples receive identical treatment under PECVD as shown in Figure S3.

The quantitative EDS results are summarized in Figure 5, which summarizes the atomic ratio of oxygen to boron as a function of the treatment time under hydrogen plasma. The rate of removal here follows a linear trend with a decrease in the O/B ratio at a rate of ~7.5×10^{-4} min^{-1}. These experiments were repeated three times and an error of ± 10% was observed in the measurement of the O/B atomic ratio.

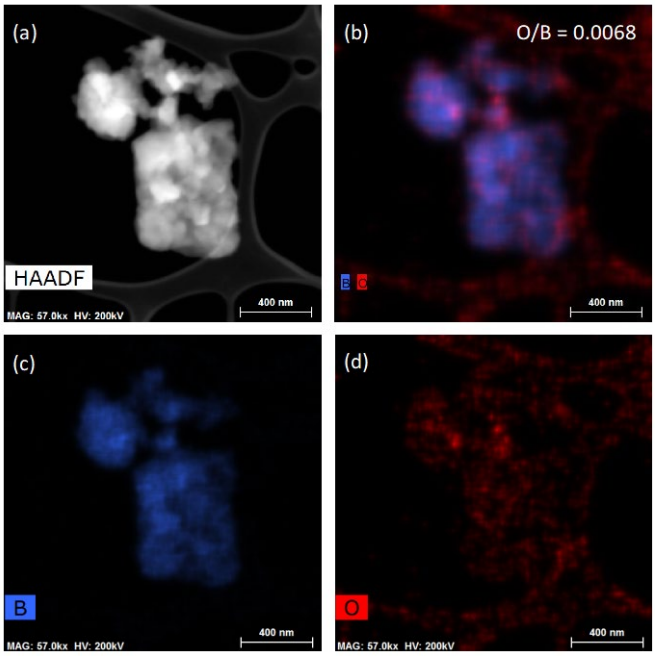

Figure 4. STEM-EDS images of BNPs in HAADF mode after 120 min hydrogen plasma treatment. (a) STEM image showing boron particles; (b) EDS image showing the relative distribution of boron (blue) and oxygen (red) on a particle (O/B = 0.0068); (c) EDS image showing individual micrograph of boron on a particle; and (d) EDS image showing individual micrograph of oxygen on a particle. Oxygen distribution seems to be significantly reduced due to the hydrogen plasma treatment of boron particles.

SEM and TEM micrographs for as-received and plasma-treated BNPs are shown in Figures 6 and 7, respectively. The SEM images of the untreated particles (Figure 6a) show extensive agglomeration. TEM micrographs in Figure 7 indicate that aggregates are formed by primary particles whose size ranges from 20 nm to 100 nm, in qualitative agreement with the nominal size of 70 nm reported by the manufacturer. Dynamic light scattering (DLS) measurements of BNPs suspended in ethanol give a mean hydrodynamic diameter of ~220 nm, in agreement with cluster sizes seen in TEM (Figure 7b). Plasma treatment does not cause any

visible change to the structure of the particles as seen in Figures 7c, 7d and 6b. Samples remain agglomerated and the size obtained by DLS remains the same.

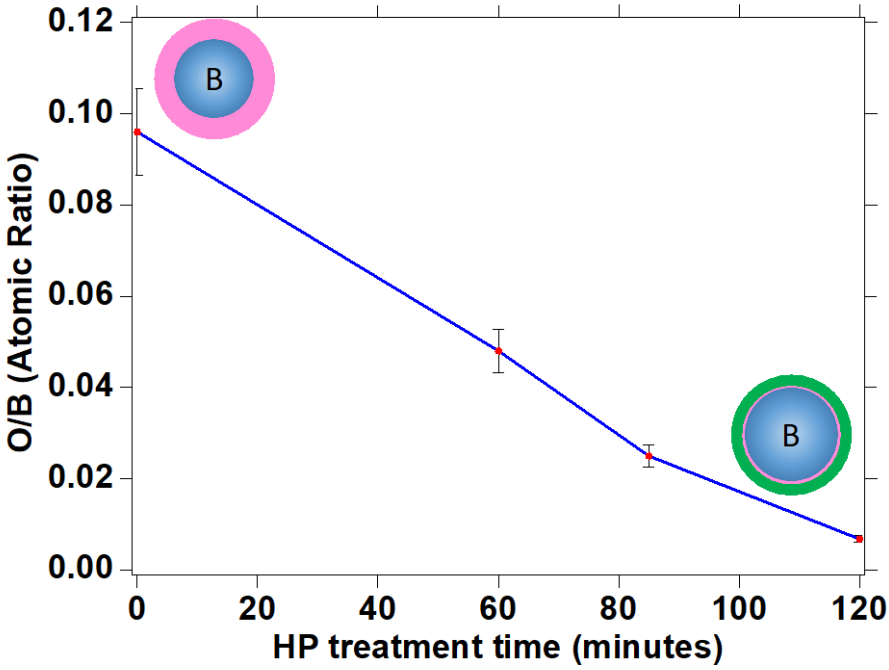

Figure 5. STEM-EDS results of O/B ratio with exposure time to the hydrogen plasma. Blue represents the boron core, pink is the oxide layer, and the green represents the PECVD coating. Bars at each point represent an error of ± 10% in measuring the O/B atomic ratio after repeating the experiments three times.

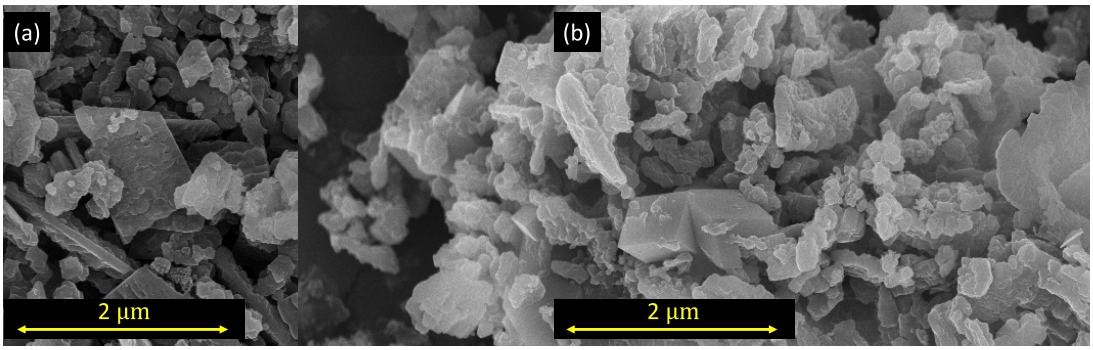

Figure 6. SEM micrographs of BNPs: (a) as received, and (b) after 120 min in hydrogen plasma followed by 15 min of PECVD.

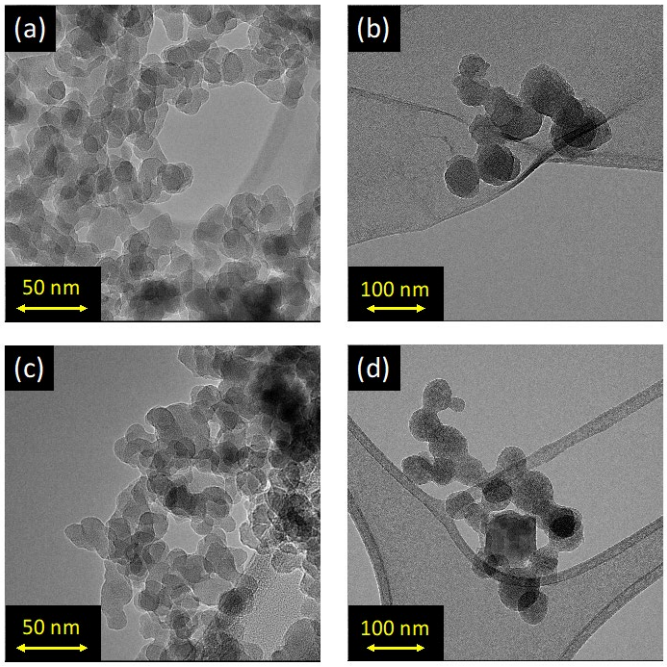

Figure 7. TEM micrographs of BNPs: (a) and (b) as received, (c) and (d) after plasma treatment (120 min in hydrogen plasma followed by 15 min of PECVD).

To probe the presence of elements and chemical bonds at the particle surface, we used X-ray photoelectron spectroscopy (XPS). XPS has a probe depth of 10-15 nm, which extends beyond the deposited PECVD film and oxide layer and into the metallic boron phase. Figure 8(a) shows the XPS survey scans of 15 min PECVD coated and 120 min hydrogen plasma-treated followed by 15 min PECVD coated BNPs. The survey scans confirm the presence of boron, carbon, oxygen and fluorine in both samples. Carbon and fluorine are due to the perfluoro-based PECVD coating on the surface while boron and oxygen are present due to metallic boron and its native oxide. Figure 8(b) shows the high-resolution C 1s spectra, which confirms the presence of C-C, C-F, CF_2, and CF_3 groups because of the 15 min PECVD treatment on the surface of BNPs. High-resolution B 1s XPS spectra are shown in Figures 8(c) and 8(d). Two oxidation states of boron were observed; the peak at 187.2 eV is assigned to elemental boron (B^0), and the peak at a binding energy of 193 eV corresponds to oxidized boron (B^{3+}). Figure 8(c) shows 15 min PECVD coated BNPs in which the near-surface concentration of oxidized boron (B^{3+}) is 12.4 ± 0.5%. After a 120 min of hydrogen plasma treatment while keeping a PECVD time of 15 min constant, oxidized boron (B^{3+}) from the

near-surface region reduced to 4.9 ± 0.5%, as shown in Figure 8(d). This is accompanied by a corresponding increase of elemental boron by ~7% (relative to the boron present in the untreated sample), which is due to the reduction of the oxide under hydrogen plasma treatment. The XPS determined trend of the reduction of the surface oxide with hydrogen plasma treatment time is presented in Figure S6 (Supporting Information).

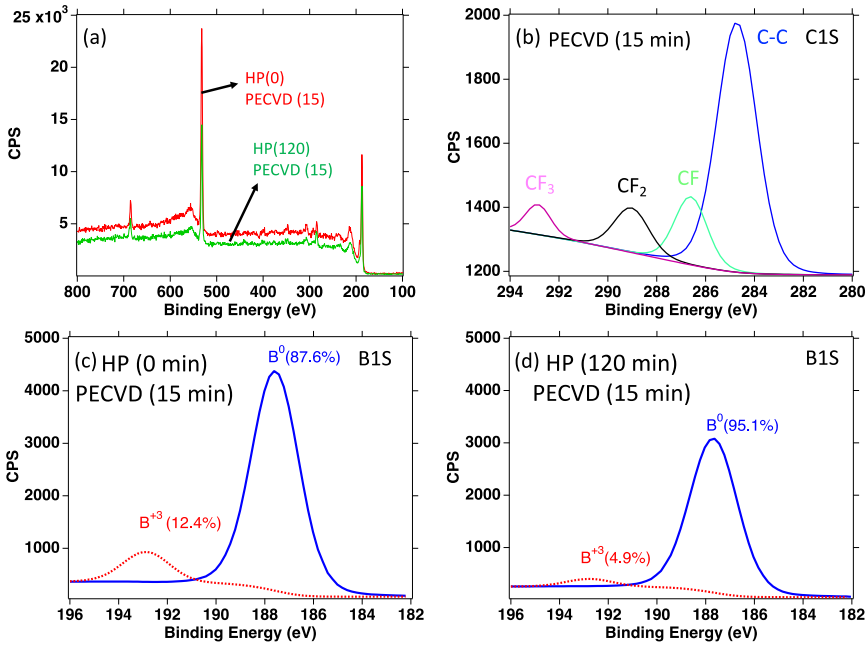

Figure 8. (a) XPS survey scans of 15 min PECVD coated and 120 min hydrogen plasma-treated followed by a PECVD application for 15 min, (b) High-resolution C 1s spectra due to PECVD application of 15 min, (c) High-resolution B 1s spectra for PECVD application for a 15 min (B^{3+} = 12.4%), (d) High-resolution B 1s spectra for a hydrogen plasma treatment for 120 min followed by PECVD application for 15 min (B^{3+} = 4.9%).

The weight gain on oxidation in the air of untreated and treated BNPs was measured by thermal gravimetric analysis (TGA). Four samples were analyzed three times each in a span of 60 days to check the storage life and to ensure the reproducibility of the results: (a) untreated BNPs, (b) 15 min PECVD treated BNPs, (c) 85 min hydrogen plasma and 15 min PECVD treated BNPs and (d) 120 min hydrogen plasma and 15 min PECVD treated BNPs. A heating rate of 30°C/min was used with a volumetric flow rate of air of 100 mL/min. Thermogravimetric profiles of the untreated BNPs and plasma-treated samples are shown in

Figure 9. The inset in Figure 9 shows in magnification the weight loss occurring in the temperature range of 20-500ºC. The low-temperature weight loss represents the decomposition of volatile impurities and hydrated B_2O_3 [37]. Volatile impurities can be ~0.5% as specified by the manufacturer.

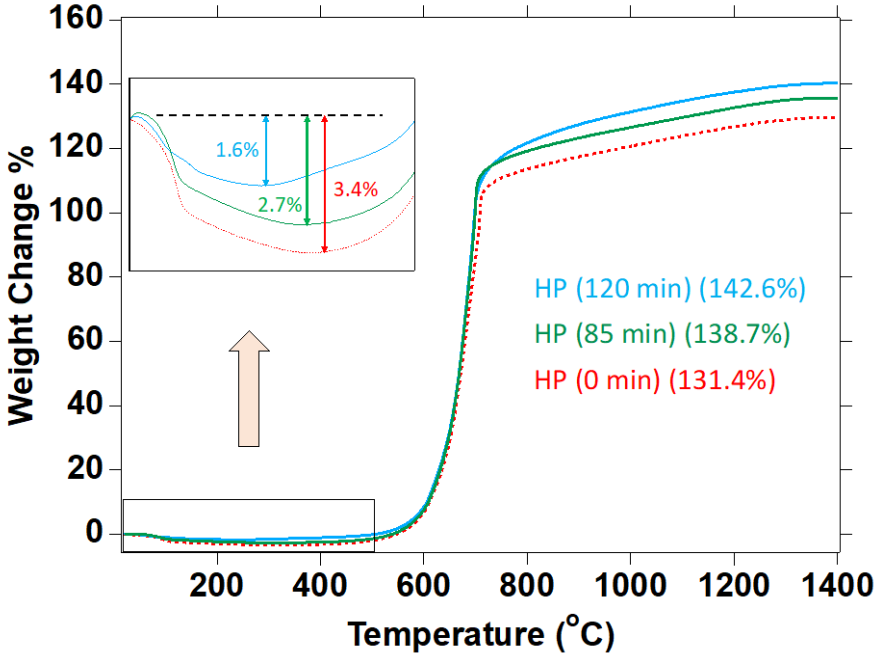

Figure 9. TGA results for untreated BNPs (dotted red) with a weight gain of 131.4%, hydrogen plasma (85 min) and PECVD (15 min) treated BNPs (green), and hydrogen plasma (120 min) and PECVD (15 min) treated BNPs (blue) with weight gain of 138.7% and 142.6%, respectively. HP is used for hydrogen plasma in the graph annotations. Weight gain % due to the oxidation of boron is given in the brackets.

In parallel with TGA, we performed differential scanning calorimetry (DSC) to measure the amount of heat released during oxidation. The DSC results are shown in Figure 10. The energy release (in kJ/g) of the BNPs is obtained by integration of the exothermic peaks as a function of time. For all samples, we observe a single exothermic peak between 580°C to 750°C with a maximum of ~650°C. This temperature range agrees with the sharp increase in weight in Figure 9. No other significant exotherm is observed, at least up to 1400 °C, which is the highest temperature of this study.

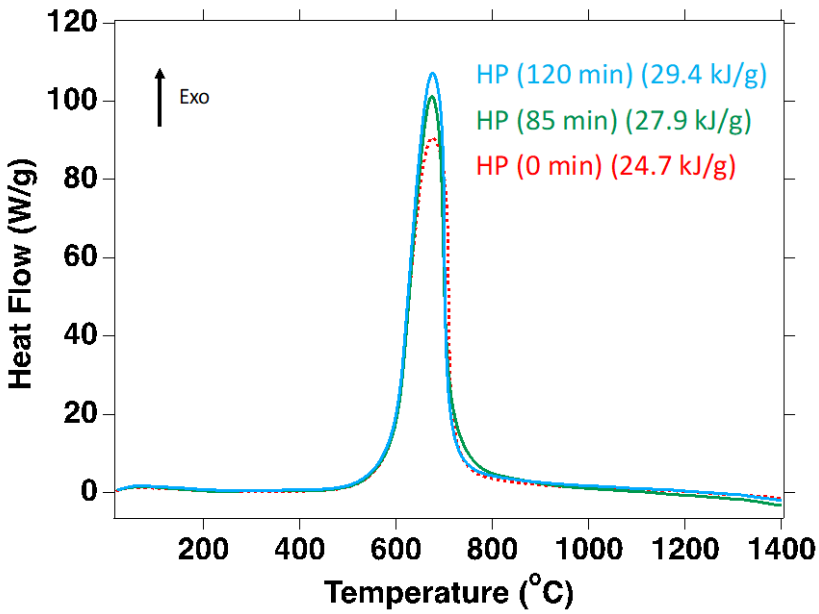

Figure 10. DSC results demonstrate a 19% increase in energy release (in kJ/g) after 120 min of hydrogen plasma treatment: Untreated BNPs (dotted red) with an energy release of 24.7 kJ/g, hydrogen plasma (85 min) and PECVD (15 min) treated BNPs (green), and hydrogen plasma (120 min) and PECVD (15 min) treated BNPs (blue) with energy release of 27.9 kJ/g and 29.4 kJ/g, respectively. HP is used for hydrogen plasma in the graph annotations. Energy release (in kJ/g) is given in parentheses, which is calculated by integrating the curves with respect to time.

Table 1: Comparison of weight gain and energy release (in kJ/g) measured from thermal analysis after different time treatments and percent increase in energy release with respect to the reference sample (Untreated BNPs)

Treatment (Time is shown in brackets in min)	**Weight Gain (%)**	**Energy Release (kJ/g) with error of ± 1%**	**% Increase in energy release with respect to the reference (untreated BNP)**
Untreated Sample	131.4	24.7	-
Hydrogen Plasma (0) PECVD (15)	131.4	25.6	+4
Hydrogen Plasma (60) PECVD (15)	135.3	27	+9.3
Hydrogen Plasma (85) PECVD (15)	138.7	27.9	+13
Hydrogen Plasma (120) PECVD (15)	142.6	29.4	+19

Table 1 summarizes the results from the thermal analysis (TGA-DSC). The as-received BNPs show the lowest gravimetric heat release as well as the lowest weight gain. Both the amount of heat released and the weight gain increase with increasing treatment time in hydrogen plasma.

4. DISCUSSION

4.1 Reduction of Native Oxide using Hydrogen Plasma

Treatment under hydrogen plasma is successful in removing the native oxide layer from the surface of BNPs. Hydrogen plasma produces reactive hydrogen species including atomic (H) and ionic hydrogen (H^+) to reduce boron oxide as shown in reactions (1) and (2) respectively [31].

$$B_2O_3\ (s) + 6H\ (g) \rightarrow 2B\ (s) + 3H_2O\ (g) \qquad (1)$$

$$B_2O_3\ (s) + 6H^+\ (g) + 6\ e^- \rightarrow 2B\ (s) + 3H_2O\ (g) \qquad (2)$$

The feasibility of a reaction is established by a negative Gibbs energy change (ΔG). The thermodynamic calculations were performed with HSC, an industrial thermodynamic software package (https://www.hsc-chemistry.com/). The data shows the negative Gibbs energy (favorable reaction) when using H and H^+, especially at low temperatures as shown in Figure 11. It is observed from the graph that molecular hydrogen (H_2) cannot reduce B_2O_3 even at high temperatures. ΔG values are positive at temperatures ranging from 0-1000ºC, which implies that the reaction of B_2O_3 with H_2 gas is not feasible at even high temperatures. Reduction of B_2O_3 at a plasma site by atomic and ionic hydrogen is possible due to the feasibility of reactions (1) and (2) at all the temperatures ranging from 0-1000ºC, as indicated by the negative ΔG shown in Figure 11. The non-thermal plasma system used in our study works at room temperature (~25ºC), causing the reduction of B_2O_3 from the surface of BNPs.

The complete thermodynamic analysis of the above mentioned reactions are shown in the Supporting Information (Table S1, S2, and S3). In addition to the thermodynamic feasibility of non-thermal hydrogen plasma, stable boron oxide is reduced because of the lower activation energy of the reactions (1) and (2) in comparison with the corresponding molecular reactions as studied by Sabat et al. [31] and others [32, 34-35]. The rate of the reaction is proportional to the exposed oxide surface, which is essentially constant during the reaction. Accordingly, the amount of oxide removed is a linear function of time (HRTEM images in Figure 2 and Figure S1) with a rate of 0.05 nm/min. This linear dependence is supported by both EDS (Figure 5) and XPS (Figure S6 in Supporting Information).

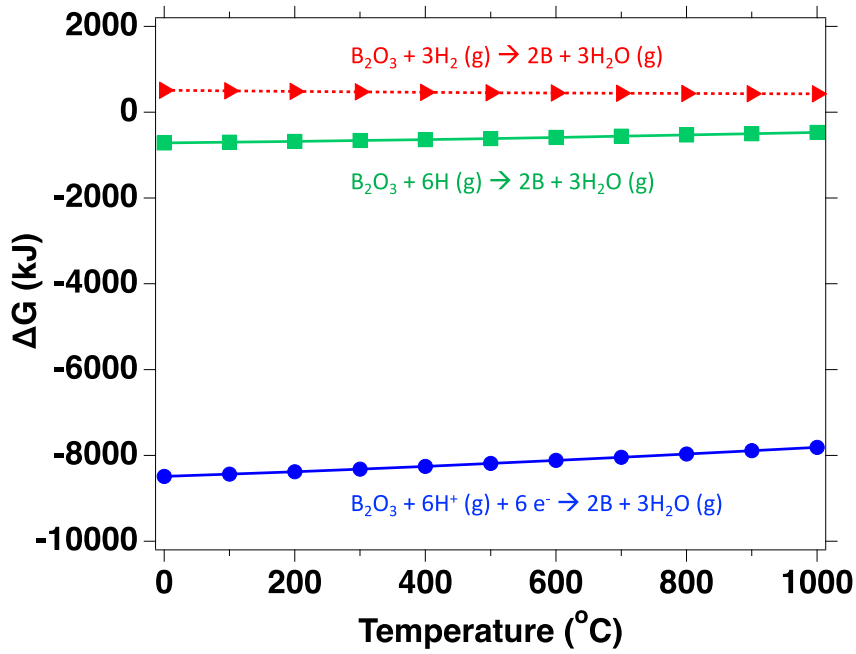

Figure 11. Gibbs energy change (ΔG) as a function of temperature is shown for molecular hydrogen (red), atomic hydrogen (green), and ionic hydrogen (blue). These results indicate that reactive hydrogen species (atomic hydrogen and ionic hydrogen) generated from hydrogen plasma can reduce boron oxide even at low temperatures.

4.2 Effect of Plasma Treatment on the Oxidation and Energetics of BNPs

The performance of nanoenergetic materials is sensitive to the degree of agglomeration. Chintersingh et al. [37] used acetonitrile with other hydrocarbons to remove the oxide layer and showed that boron under TGA oxidizes more completely when less agglomerated. As a

dry, low-temperature process, plasma processing does not induce agglomeration. Agglomeration could increase due to passivation coating if multiple clusters are encapsulated by the depositing film as a single unit. This is not the case here. As Figures 6 and 7 indicate, the degree of agglomeration before and after plasma processing is the same and is limited by the quality of the starting material.

The removal of the oxide layer and improvement in the oxidation characteristics are further confirmed by TGA. The weight gain in the TGA experiments (Figure 9) is due to the formation of the oxide and indicates the amount of boron oxidized under TGA test conditions. The low-temperature weight loss [37] is the highest (3.4%) for untreated BNPs because of the presence of a thicker hydrated B_2O_3 layer and it reduces to 1.6% after 120 min of hydrogen plasma treatment as shown in Figure 9. A sharp decrease near 100°C is due to dehydration and the blunt decrease after that is because of the decomposition of other volatile impurities. The decreasing magnitudes of both the overall weight loss and the weight loss due to dehydration from hydrated B_2O_3 (sharp decrease) suggest the substantial reduction of hydrated B_2O_3 from the surface of BNPs as a result of hydrogen plasma treatments.

The weight gain is lowest for untreated BNPs and increases systematically with treatment time under hydrogen plasma (Table 1). A corresponding increase is observed in the heat flow measured by DSC (Table 1 and Figure 10). Interestingly, a sample with only 15 min PECVD treatment has the same weight gain in TGA as the untreated boron sample, but the energy released in the DSC measurement is ~4% higher than the untreated BNPs. The additional energy release of ~4% (1 kJ/g) can occur as a result of exothermic gasification of B_2O_3 [51-54] into BF_3 due to the presence of perfluoro-based plasma films on the surface (CF_x) as evident by XPS analysis in Figure 8. The gasification of B_2O_3 results in enhancing the contact between the oxidizer and boron, due to which some extra boron oxidizes to B_2O_3. This gasification leads to a weight loss of the sample but that could be counteracted by the weight

gain caused by the oxidation of extra boron (or previously unexposed boron surface). The balance between the weight loss due to gasification of B_2O_3 and the weight gain as a result of additional oxidation of boron in the same temperature range could be the possible reason for similar weight gains for the untreated sample and the PECVD-only treated sample as shown in Table 1.

BNPs treated for 120 min show a weight gain that is 11.2% higher than the untreated BNPs. This is accompanied by a 19% increase in the energy release (from 24.7 kJ/g to 29.4 kJ/g). Stoichiometric calculations using equation S8 (Supporting Information) demonstrate an 11.2% weight gain corresponds to the oxidation of an additional 5% metallic boron in thermal analysis. This extra 5% metallic boron content improves the energy release by ~15% (3.6 kJ/g), caused by the additional metal oxidation as well as the better interfacial contact between an oxidizer and boron due to the reduced concentration of B_2O_3 after hydrogen plasma treatment.

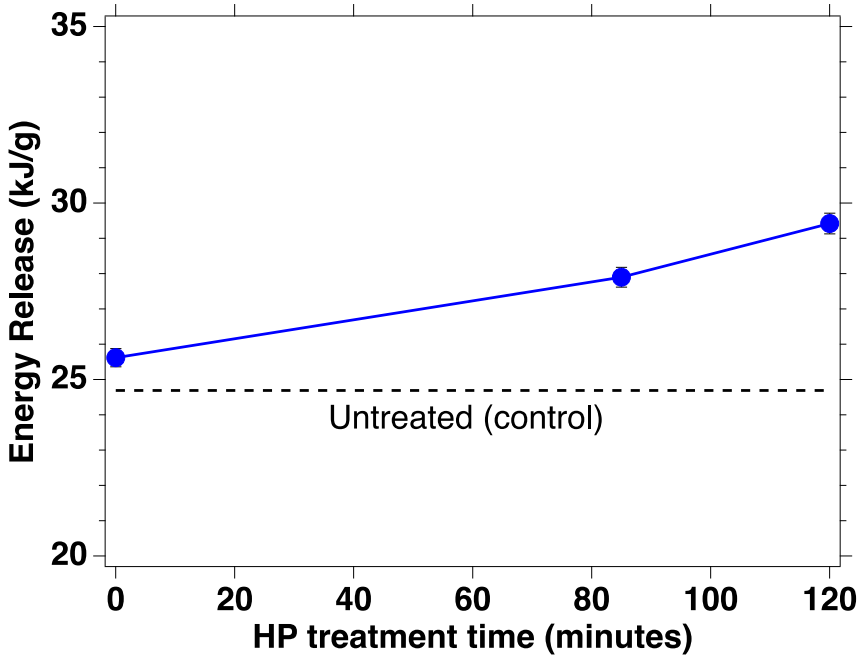

Figure 12. Energy release (kJ/g) measured by DSC as a function of hydrogen plasma treatment time (error bars: ± 1%). The plot shows a linear trend in the improvement of the energy release of BNPs with respect to hydrogen plasma treatment time. The dotted reference line shows the energy release of untreated BNPs (control sample). The difference between the dotted reference line and the first data point at time, t = 0 min is energy release associated with the oxidation of the perfluoro-based PECVD films.

The increase in energy release occurs due to the reduction of the oxide layer which eliminated the diffusion barrier for the oxidizer to access a greater volume fraction of metallic boron in the BNPs. No significant exothermic peak is observed after ~750°C because of the presence of liquid boron oxide that clogs the porosity as the oxidation reaction progresses [50]. This decreases the overall rate of oxidation of the boron sample. Figure 12 shows a linear trend in the improvement of energy released from BNPs with respect to hydrogen plasma treatment time, thereby concluding that improvement in the energy release and reduction in oxide (Figure S6 in Supporting Information and Figure 5) follow linear trends, and this confirms that energy release and surface oxide reduction are correlated with each other.

4.3 Perfluoro-based PECVD Passivation

The deposition of the PFD coating following the removal of the oxide layer is critical for maintaining the reduced state of the particle surface. A thickness of 2.5 nm as shown in Figure 2 effectively passivates particles against oxidation during storage and subsequent analyses. EDS also confirms that the coating shown in Figure 2 by HRTEM analysis is composed of the CF_x, which can provide a hydrophobic barrier [40] for the BNPs. (Figure S10 in Supporting Information). Plasma-based perfluorocarbon coatings exhibit very good stability over time. TGA-DSC measurements of plasma-treated BNPs performed after 60 days of storage under ambient conditions show no significant change compared to an untreated sample (Figure S9 in Supporting Information).

A further advantage of the presence of fluorine at the particle surface is an additional contribution to the energy release of the order of 4% (25.6 kJ/g from DSC analysis) as compared to the untreated BNPs (control) (24.7 kJ/g from DSC analysis). The PECVD coating containing CF_x triggers their exothermic reaction with boron oxide (formed due to oxidation by air) to form gaseous boron fluoride that increases the apparent enthalpy near the oxidation

temperature of boron (~600ºC) [52]. This effect has been reported in several studies of perfluoro-based coatings [38, 51] and fluorocarbon additives (though not by plasma) to the combustion of metal oxides [52-55]. In other studies [11-14, 26, 28], surface films formed from alkoxy groups, halogens, silanes, oleic acid by solution-based methods adversely affect the heat release from BNPs because they do not react chemically with the boron oxide and the elements present on the surface have much lower energy density compared to boron. The presence of fluorocarbon on the surface is therefore important, not only for providing passivation but also for its combustion chemistry [52]. DSC results in this paper also suggest a possibility that fluorocarbon-based plasma films can improve the energy release from BNPs.

5. CONCLUSIONS

We developed an *in-situ* non-thermal plasma processing method to produce BNPs with improved energetic performance and storage life. We found non-thermal hydrogen plasma produced reactive species of hydrogen which reduced the oxidized boron surface. PECVD processing after the reduction of the oxide prevents the re-oxidation of the surface while improving the storage life of the BNPs in ambient conditions. HR-TEM, STEM-EDS, and XPS were used to characterize the oxide reduction both qualitatively and quantitatively. The reduction in native oxide content correlates with the thermal analysis results, which display an increase in active boron content and energy release of the hydrogen plasma-treated samples. The native oxide layer is a diffusion barrier and upon reduction of this barrier, leading to an increase in the fraction of metallic boron, a 19% higher energy release was observed during oxidation in air. Passivation by PECVD increased the storage time of the BNPs since we observed no changes in the measured energy release over 60 days. We conclude non-thermal plasma processing is a highly attractive technique to improve the performance of advanced nanoenergetic materials.

AUTHOR INFORMATION

*Corresponding author – Themis Matsoukas

E-mail address: txm11@psu.edu; Tel.: +1-814-863-2002

ORCID

Prawal Agarwal: 0000-0002-8795-6077

Devon Jensen: 0000-0001-5890-3972

Chien-Hua Chen: 0000-0002-2936-9528

Robert Rioux: 0000-0002-6019-0032

Themis Matsoukas: 0000-0002-0097-2673

ACKNOWLEDGMENTS

This work was supported by DOD SBIR under contract number N68936-19-C-0015. We gratefully acknowledge support from the United States Navy (Dr. Ben Harvey) and Advanced Cooling Technologies (ACT). We are also thankful to the Material Characterization Lab (MCL) at Pennsylvania State University, where the material characterization experiments have been performed.

Supporting Information Available

The supporting information is available free of charge.

HR-TEM, STEM-EDS, XPS, and TGA-DSC results for the remaining samples. Calculation of active boron content from TG results. DSC results for the samples stored for 60 days. EDS micrograph showing F distribution on boron particle. Differential TG results before and after plasma treatment. Thermodynamic analysis of hydrogen plasma reduction of B_2O_3.

Financial Interest Statements

The authors declare no conflict of interest.

REFERENCES

[1] Chung, H.S.; Chen, C.S.H.; Kremer, R.A.; Boulton, J.R.; Burdette, G.W. "Recent Developments in High-energy Density Liquid Hydrocarbon Fuels", Energy & Fuels 1999, 13, 641–649.

[2] Hui, X.; Kumar, K.; Sung, C.J.; Edwards, T.; Gardner, D. "Experimental Studies on the Combustion Characteristics of Alternative Jet Fuels", Fuel 2012, 98,176–182.

[3] Dreizin, E.L. "Metal-based Reactive Nanomaterials", Progress in Energy and Combustion Science 2009, 35(2), 141–167.

[4] Yetter, R.A.; Risha, G.A.; Son, S.F. "Metal Particle Combustion and Nanotechnology", Proceedings of Combustion Institute 2009, 32, 1819-1838.

[5] Beach, D.B.; Rondinone, A.J.; Sumpter, B.G.; Labinov, S.D.; Richards, R.K. "Solid-state Combustion of Metallic Nanoparticles: New Possibilities for an Alternative Energy Carrier", J. Energy Resour. Technol. 2007, 29.

[6] Bergthorson, J.M. "Recyclable Metal Fuels for Clean and Compact Zero-carbon Power", Progress in Energy & Combustion Science, Vol 68, 2018, 169-196.

[7] Mandilas, C.; Karagiannakis, G.; Konstandopoulos, A.G.; Beatrice, C.; Lazzaro, M.; Di Blasio, G.; Molina, S.; Pastor, J.V.; Gil, A. "Study of Basic Oxidation and Combustion Characteristics of Aluminum Nanoparticles under Enginelike Conditions", Energy Fuels 28 (2014) 3430–3441.

[8] Shkolnikov, E.I.; Zhuk, A.Z.; Vlaskin, M.S. "Aluminum as Energy Carrier: Feasibility Analysis and Current Technologies Overview", Renew. Sustain. Energy Rev. 15 (2011) 4611–4623.

[9] Wen, D. "Nanofuel as a Potential Secondary Energy Carrier", Energy Environ. Sci. 3, (2010) 591–600.

[10] Ojha, P. K.; Karmakar, S. "Boron for Liquid Fuel Engines - A Review on Synthesis, Dispersion Stability in Liquid Fuel, and Combustion Aspects", Progress in Aerospace Sciences,100, 2018, 18-45.

[11] Yu, W.; Xie, H. "A Review on Nanofluids: Preparation, Stability Mechanisms, and Applications", J. Nanometer. 2012, 1–17.

[12] Rao, D. Srinivas; Dash, R.K. "Effect of Nanomaterials Sizes on the Dispersion Stability of Biodiesel-based Nanofluids", Adv. Mater. Lett. 6 (2015) 247–251.

[13] Ghadimi, A.; Saidur, R.; Metselaar, H.S.C. "A Review of Nanofluid Stability Properties and Characterization in Stationary Conditions", Int. J. Heat Mass Tran. 54 (2011) 4051–4068.

[14] Van Devener, B.; Perez, J.P.L.; Jankovich, J.; Anderson, S.L. "Oxide-free, Catalyst-coated, Fuel-soluble, Air-stable Boron Nanopowder as Combined Combustion Catalyst and High Energy Density Fuel", Energy Fuel 2009, 23:6111–6120.

[15] Li, X.; Wang, X.; Zhang, J. “Hollow Boron Nitride Nanospheres as Boron Reservoir for Prostate Cancer Treatment”, Nat Commun 8, 2017, 13936.

[16] Mortensen, M.W.; Sorensen, P.G.; Bjorkdahl, O.; Jensen, M.R.; Gundersen, H.J.G.; Bjornholm, T. “Preparation and Characterization of Boron Carbide Nanoparticles for Use as a Novel Agent in T cell-guided Boron Neutron Capture Therapy”. Appl Radiat Isotopes 2006, 64:315–324.

[17] Bekish, Y.N.; Poznyak, S.K.; Tsybulskaya, L.S.; Gaevskaya, T.V. “Electrodeposited Ni–B Alloy Coatings: Structure, Corrosion Resistance and Mechanical Properties”. Electrochim Acta 2010, 55:2223–2231.

[18] Blase, X.; Bustarret, E.; Chapelier, C. “Superconducting Group-IV Semiconductors”, Nature Mater 8, 2009, 375–382.

[19] Shyu, I.M.; Liu, T.-K. “Combustion Characteristics of GAP-coated Boron Particles and the Fuel-rich Solid Propellant”, Combust. Flame 100 (1995) 634–644.

[20] Liu, J.Z.; Xi, J.F.; Yang, W.J.; Hu, Y.R.; Zhang, Y.W.; Wang, Y.; Zhou, J.H. “Effect of Magnesium on the Burning Characteristics of Boron Particles”, Acta Astronaut. 96 (2014) 89–96.

[21] Xi, J.; Liu, J.; Wang, Y.; Liang, D.; Zhou, J. “Effect of Metal Hydrides on the Burning Characteristics of Boron”, Thermochim. Acta 597 (2014) 58–64.

[22] Spalding, M.J.; Krier, H.; Burton, R.L. “Boron Suboxides Measured during Ignition and Combustion of Boron in Shocked Ar/F/O2 and Ar/N2/O2 Mixtures”, Combust. Flame 120 (2000) 200–210.

[23] Krier H.; Burton, R.L.; Spalding, M.J.; Rood, T.J. “Ignition Dynamics of Boron Particles in a Shock Tube”, J. Propul. Power 14 (1998) 166–172.

[24] Matsko, A.M.; Zolotko, A.N. “The Ignition of Boron-Magnesium Dust Clouds”, 1989.

[25] Rosenband, V.; Natan B.; Gany, A. “Ignition of Boron Particles Coated by a Thin Titanium Film”, J. Propul. Power 11 (1995) 1125–1131.

[26] Bellott, B.J.; Noh, W.; Nuzzo, R.G.; Girolami, G.S. “Nanoenergetic Materials: Boron Nanoparticles from the Pyrolysis of Decaborane and their Functionalization”. Chem Commun 2009, 22:3214–3215.

[27] Marzik, J.V.; Suplinskas, R.J.; Wilke, R.H.T.; Canfield, P.C.; Finnemore, D.K.; Rindfleisch, M.; Margolies, J.; Hannahs, S.T. “Plasma Synthesized Doped B Powders for MgB2 Superconductors”. Physica C 2005, 423:83–88.

[28] Pickering, A.L.; Mitterbauer, C.; Browning, N.D.; Kauzlarich, S.M.; Power, P.P. “Room Temperature Synthesis of Surface Functionalised Boron Nanoparticles”. Chem Commun 2007, 6:580–582.

[29] Si, P.Z.; Zhang, M.; You, C.Y.; Geng, D.Y.; Du, J.H.; Zhao, X.G.; Ma, X.L.; Zhang, Z.D. "Amorphous Boron Nanoparticles and BN Encapsulating Boron Nano-peanuts Prepared by Arc-decomposing Diborane and Nitriding". J Mater Sci 38:689–692, 2003

[30] Shin, W.G.; Calder, S.; Ugurlu, O.; Girshick, S.L. "Production and Characterization of Boron Nanoparticles Synthesized with a Thermal Plasma System", J Nanopart Res (2011) 13:7187–7191

[31] Sabat, K.C.; Rajput, P.; Paramguru, R.K.; Bhoi, B.; Mishra, B.K. "Reduction of Oxide Minerals by Hydrogen Plasma: An Overview", Plasma Chem Plasma Process 34:1–23, 2014

[32] Meichsner, J.; Schmidt, M.; Schneider, R.; Wagner, H. "Nonthermal Plasma Chemistry and Physics", CRC Press, 2013

[33] Zhang, X.W.; Zou, Y.J.; Yan, H.; Wang, B.; Chen, G.H.; Wong, S.P. "Electrical Properties and Annealing Effects on the Stress of RF-sputtered c-BN Films", Mater Lett 45:111–115, 2000

[34] Yasushi, S.; Tamaru, H.; Kogoma, M.; Kawase, M.; Hashimoto, K. "The Reduction of Copper Oxide Thin Films with Hydrogen Plasma Generated by an Atmospheric-pressure Glow Discharge", J. Phys. D: Appl. Phys. 29 2539, 1996

[35] Chang, R.P.H.; Chang, C.C.; Darack, S. "Hydrogen Plasma Etching of Semiconductors and their Oxides", Journal of Vacuum Science and Technology 20, 45, 1982

[36] Nishiyama, I.; Oizumi, H.; Motai, K. "Reduction of Oxide Layer on Ru Surface by Atomic-hydrogen Treatment", Journal of Vacuum Science & Technology B: Microelectronics and Nanometer Structures Processing, Measurement, and Phenomena 23, 3129, 2005

[37] Chintersingh, Kerri-Lee; Schoenitz, M.; Dreizin, E.L. "Oxidation Kinetics and Combustion of Boron Particles with Modified Surface", Combustion and Flame, Volume 173, 2016, Pages 288-295.

[38] Valluri, S.K.; Schoenitz, M.; Dreizin, E.L. "Bismuth fluoride-coated Boron Powders as Enhanced Fuels", Combustion and Flame, Volume 221, 2020, Pages 1-10.

[39] Vasudev, M.C.; Anderson, K.D.; Bunning, T.J.; Tsukruk, V.V.; Naik, R.R. "Exploration of Plasma-enhanced Chemical Vapor Deposition as a Method for Thin Film Fabrication with Biological Applications", ACS Applied Materials & Interfaces, 5, 3983-3994, 2013

[40] Shahravan, A., Desai, T., Matsoukas, T. "Passivation of Aluminum Nanoparticles by Plasma-enhanced Chemical Vapor Deposition for Energetic Nanomaterials", ACS Applied Materials & Interfaces, vol. 6, no. 10, pp. 7942–7947, 2014

[41] Zhou, X.; Torabi, M.; Lu, J.; Shen, R.; Zhang, K. "Nanostructured Energetic Composites: Synthesis, Ignition/Combustion Modeling, and Applications". ACS Appl. Mater. Interfaces 2014, 6, 3058−3074.

[42] Huang, Y.; Risha, G. A.; Yang, V.; Yetter, R. A. "Effect of Particle Size on Combustion of Aluminum Particle Dust in Air". Combust. Flame 2009, 156, 5−13.

[43] Cao, J.; Matsoukas, T. “Nanoparticles and Nanocomposites in RF Plasma”. Mater. Res. Soc. Symp. 2001, 635, c.4.12.1−c.4.12.6.

[44] Cao, J.; Matsoukas, T. “Deposition Kinetics on Particles in a Dusty Plasma Reactor”. J. Appl. Phys. 2002, 92, 2916−2922.

[45] Shahravan, A.; Desai, T.; Matsoukas, T. “Controlled Manipulation of Wetting Characteristics of Nanoparticles with Dry-based Plasma Polymerization Method”. Applied Physics Letters, vol. 101, no. 25, Article ID 251603, 2012

[46] Chen, Z.; Ren, W.; Gao, L. “Three-dimensional Flexible and Conductive Interconnected Graphene Networks Grown by Chemical Vapour Deposition.” *Nature Mater* 10, 424–428, 2011

[47] Matsoukas, T.; Cao, J. “Film Deposition on Particles Trapped in the Sheath of Reactive Dusty Plasma: Effect of Size Distribution”. Plasma Science, IEEE Transactions on, 32(2):699 – 703, April 2004.

[48] Cao, J.; Matsoukas, T. “Synthesis of Hollow Nanoparticles by Plasma Polymerization”. Journal of Nanoparticle Research, 6(5):447–455, 10 2004.

[49] Seah, M.P. “Summary of ISO/TC 201 Standard: VII ISO 15472:2001 — Surface Chemical Analysis — X-ray Photoelectron Spectrometers — Calibration of Energy Scales”, Surf. Interface Analysis 31 721-723, 2001

[50] Sun, Y.; Chintersingh, Kerri-Lee; Schoenitz, M.; Dreizin, E.L. “Reactive Shell Model for Boron Oxidation”, The Journal of Physical Chemistry C 2019 123 (18), 11807-11813.

[51] McCollum, J.; Pantoya, M.L.; Iacono, S.T. “Activating Aluminum Reactivity with Fluoropolymer Coatings for Improved Energetic Composite Combustion”, ACS Appl. Mater. Interfaces, 7, 33, 18742-18749. 2015

[52] Yetter, R. A.; Dryer, F. L.; Rabitz, H.; Brown, R. C.; Kolb C. E. “Effect of Fluorine on the Gasification Rates of Liquid Boron Oxide Droplets,” Combustion and Flame, 112 387-403, 1998

[53] Jiang, Y.; Deng, S.; Hong, S.; Tiwari, S.; Chen, H.; Nomura, K.; Kalia, R.K.; Nakano, A.; Vashishta, P.; Zachariah, M.R.; Zheng, X. “Synergistically Chemical and Thermal Coupling between Graphene Oxide and Graphene Fluoride for Enhancing Aluminum Combustion”, ACS Applied Materials & Interfaces, 12 (6), 7451-7458. 2020

[54] Ulas, R.; Kuo, K. K.; Gotzmer, C. “Ignition and Combustion of Boron Particles in Fluorine-Containing Environments”, Combustion and Flame, 127 1935-1957, 2001

[55] Zhou, W.; Yetter, R. A.; Dryer, F. L.; Rabitz, H.; Brown, R. C.; Kolb, C. E. “Effect of Fluorine on the Combustion of “Clean” Surface Boron Particles,” Combustion and Flame, 112 507-521, 1998